On the possible contribution of cationic oxygenated carbon chains C n O+, HC n O+, and OC n O+ (n = 4 – 9) to the diffuse interstellar bands

U Jacovella, Jack Buntine, Mariah Cotter, Giel Muller, Michael Scholz, Emmanuel Dartois

On the possible contribution of cationic oxygenated carbon chains C_nO^+, HC_nO^+, and OC_nO^+ ($n = 4 - 9$) to the diffuse interstellar bands

U. Jacovella,[1]★ Jack T. Buntine,[2] Mariah Cotter,[2] Giel Muller,[2] Michael S. Scholz,[3] and Emmanuel Dartois[1]

[1] *Université Paris-Saclay, CNRS, Institut des Sciences Moléculaires d'Orsay, 91405 Orsay, France*
[2] *School of Chemistry, The University of Melbourne, Victoria 3010, Australia*
[3] *Department of Chemistry, University College London, 20 Gordon Street, London WC1H 0AJ, United Kingdom*

Accepted XXX. Received YYY; in original form ZZZ

ABSTRACT

Only 4 of the diffuse interstellar bands (DIBs) are currently accounted for, ascribed to electronic transitions of C_{60}^+. Investigations into carriers of other DIBs historically focus on charged and neutral hydrocarbons, and little information is available regarding oxygenated carbon and hydrocarbon species that result from the two most abundant heavy elements in the interstellar medium, C and O. In this study, we assess whether C_nO^+, HC_nO^+, and OC_nO^+ ($n = 4 - 9$) cations are viable candidates to account for DIBs using both density-functional theory (DFT) and coupled cluster single-double and perturbative triple theory, CCSD(T). For these species, the linear structures are the most stable isomers with the lowest dissociation threshold corresponding to CO loss. Optical absorptions of the oxygenated carbon chain cations are characterized by calculated vertical excitation wavelengths and their corresponding oscillator strengths using the equation-of-motion CCSD (EOM-CCSD) method. Aside from HC_4O^+ and $HC_{2n+1}O^+$, all of the species considered in this study have calculated electronic transitions that lie in the visible or near-infrared spectral regions. Minimal column densities necessary for these cations to account for DIBs have been estimated. Based on present results and the known column densities for neutral oxygenated carbon chains in TMC-1, the growth rate of charged O-bearing carbon chains *via* ion-neutral reaction mechanisms is judged to be too low to form a sufficient population to give rise to DIBs.

Key words: ISM: molecules – ISM: lines and bands – astrochemistry

1 INTRODUCTION

Identifying carriers of the diffuse interstellar bands (DIBs) remains a long-standing problem. Long carbon chains (Douglas 1977), fullerenes (Kroto & Jura 1992), and polycyclic aromatic hydrocarbons (PAHs) (Van der Zwet & Allamandola 1985) have been proposed as potential DIBs carriers, based on their likely formation, ability to withstand harsh conditions, and absorption of visible and near-infrared (NIR) light. To date, the only known carrier of DIBs is C_{60}^+ (Foing & Ehrenfreund 1994; Campbell et al. 2015), confirming that ionized carbonaceous molecules can give rise to these elusive bands. Less explored, however, is the prospect that the carriers contain other heavy elements such as O and N.(Snow & McCall 2006; Sarre 2019)

Oxygen is the most abundant heavy element in the interstellar medium (ISM), yet molecular and atomic oxygen cause continuing problems in modelling the chemistry within molecular clouds, with a compelling question brought forward: why is the atomic oxygen depleted? (Bergin et al. 2000; Goldsmith et al. 2000; Larsson et al. 2007; Quan et al. 2008; Wirström et al. 2016; Jenkins 2009; Whittet 2010; Hincelin et al. 2011). It is possible that a large portion (up to 50 %) of the depleted oxygen in molecular clouds exists in silicates and metal oxides, which are the next most abundant O-bearing species after CO and O (Whittet 2010). Hincelin et al. (2011) proposed that oxygenated carbonaceous species could also balance the oxygen budget in molecular clouds. A fraction of such matter may exist in the form of small icy grains, where the composition and abundances of major simple ices such as H_2O, CO, and CO_2 are well characterized (Dartois 2005; Öberg et al. 2011; Noble et al. 2013; Boogert et al. 2015). The composition and diversity of gaseous oxygenated carbon molecules are less understood (Herbst & Van Dishoeck 2009). Oxygen bearing carbon-rich molecules, such as oxygen-terminated carbon chains (Hardy et al. 2016), are thus promising candidates for gaseous molecules participating to the oxygen budget. In the context of the DIBs, the cationic oxygenated carbon chains are of particular interest.

Several oxygen-terminated carbon chains have been detected in space (C_2O, HC_2O, C_3O, HC_3O, HC_3O^+, C_5O, HC_5O, and HC_7O) using radio-astronomy (Matthews et al. 1984; Ohishi et al. 1991; Agúndez, Marcelino and Cernicharo, José and Guélin, Michel 2015; Palumbo et al. 2008; Cernicharo, J. et al. 2020; McGuire et al. 2017; Cordiner et al. 2017; Cernicharo et al. 2021). Searches for additional oxygenated carbon chains have been conducted based on astrochemical models, which predict observable column densities (Cordiner & Charnley 2012) using available experimental and theoretical data (Eichelberger et al. 2007; Yang et al. 2010). It is currently unclear why species such as HC_4O, HC_4O, HC_6O, C_6O, and C_7O have not been detected where they have been sought, including in the pro-

★ E-mail: ugo.jacovella@universite-paris-salcay.fr

totypical dense cloud TMC-1 (McGuire et al. 2017; Cordiner et al. 2017; Cernicharo, J. et al. 2020; Cernicharo et al. 2021). Mechanisms for the formation and destruction of most O-bearing carbon chains are not known; the detection of key carbon chain oxide molecules in the diffuse ISM would provide insights into whether these types of structures can form and survive in photo-dominated regions (PDRs) (Pety et al. 2012; Cuadrado et al. 2017). Naturally, diffuse interstellar regions are not optimal media for molecular growth through ion-neutral reactions in virtue of their quasi-collisionless conditions and high flux of UV photons and cosmic rays. Nevertheless, formation of HC_nO^+ could be envisaged by insertion of O^+ into C_nH, or the reaction between $C_{n-1}H$ and CO^+ (Chakraborty et al. 2016). Alternatively, the charge could be carried by carbon chains such as C_n^+, which react with O to give C_nO^+ or C_nH^+ with CO, ultimately forming $HC_{n+1}O^+$ (Bohme et al. 1987; Blanksby & Bowie 1999).Some of these ion–molecule reactions have been recently tested but failed to explain the observed abundances of O-bearing molecules in TMC-1.Cernicharo et al. (2021) It was proposed that radical-radical mechanisms may play a role in the formation of such species. Although $O^{(+)}$ and $CO^{(+)}$ have been detected in diffuse clouds, cationic carbon chains and neutral carbon chains longer than C_3 have not been observed. This does not preclude their presence in diffuse molecular clouds, as the difficulties to detect them could arise from their transient nature and/or their weak spectral signatures (Nagarajan & Maier 2010).

Infrared and optical spectroscopic data for C_nO^+, HC_nO^+, and OC_nO^+ are scarce, inhibiting their detection in the diffuse ISM. Electronic absorption spectra of C_7O^+ and HC_7O^+, recorded in neon matrices by the Maier laboratory (Chakraborty et al. 2016; Joseph et al. 2013), exhibit strong UV transitions with origin bands located at 276.0 nm and 278.0 nm, respectively. These absorptions are outside the spectral region of currently known DIBs. The first gas phase electronic spectra of oxygenated carbocation chains were recorded in a subsequent study by Hardy et al. (2016). Spectra of linear OC_4O^+ and a planar $HCCC(CO)CCH^+$ isomer were obtained by monitoring CO loss upon resonant laser excitation in a cryogenic 22-pole RF ion trap. The origin bands of the transitions of OC_4O^+ and of $HCCC(CO)CCH^+$ were determined to be 417.31(1) nm and 523.49(1) nm, respectively. However, these transitions could not be matched with any known DIBs, bringing into question their possible formation routes and their photostabilities in the diffuse ISM. Indeed, the CO group imposes a considerable constraint on the photostability of oxygenated carbocations in the ISM compared to hydrocarbons,Chen et al. (2018) with cumulenic-type structures such as $H_2C_{2n+1}O^+$ and $OC_{2n+1}O^+$ (with $n = 2, 3, ...$) being more stable than polyynic-type structures (Hardy et al. 2016). Combined experimental studies of infrared (IR) photodissociation spectroscopy and theoretical modelling (Jin et al. 2017; Li et al. 2019) have shown that $HC_{2n+1}O^+$ and $HC_{2n}O^+$ ($n = 3 - 6$) possess a polyyne-like carbon chain structure with closed-shell singlet ground states and cumulene-like carbon chain structures with triplet ground states, respectively. Additionally, these studies have provided a preparative method of gaseous oxygenated carbon chains using laser vaporization of a graphite target in expansion of helium seeded with a mixture of CO, H_2, and C_2H_2.

In this article, we present a computational investigation into the thermodynamic stabilities and UV/VIS absorptions of the cationic oxygenated carbon chains C_nO^+, HC_nO^+, and OC_nO^+ with $n = 4 - 9$. Possible formation mechanisms are briefly discussed. Column densities and fractions of the interstellar carbon reservoir necessary for these species to account for weak DIBs (equivalent width of 10 mÅ/mag) are estimated. This work provides a background to guide future laboratory studies and helps to identify or eliminate cationic oxygenated carbon chains as DIB carriers.

2 COMPUTATIONAL METHODS

Calculations were performed using the Gaussian 16 software suite (Frisch et al. 2016). Optimized geometries, harmonic vibrational frequencies, and scans of potential energy surfaces were calculated using density-functional theory at the ωB97X-D/cc-pVDZ level of theory (Chai & Head-Gordon 2008; Dunning 1989). Reported bond dissociation and ionization energies (BDEs; IEs) include zero-point vibrational energies at the ωB97X-D/cc-pVDZ level and single-point energies using coupled-cluster (CC) theory, with single and double excitations augmented by a perturbative treatment for estimating the effects of triple excitations (Riplinger et al. 2013) (together denoted as CCSD(T)/cc-pVTZ//ωB97X-D/cc-pVDZ) unless otherwise specified. Vertical excitation wavelengths were calculated at the EOM-CCSD/cc-pVTZ level of theory (Kowalski & Piecuch 2001; Kucharski et al. 2001).

3 STRUCTURE, ADIABATIC IONIZATION, AND DISSOCIATION ENERGIES

The possible formation and destruction of cationic oxygenated carbon chains in the diffuse ISM can be informed by the electronic structure, lowest bond dissociation energies (BDEs), and ionization energies (IEs). These have been predicted for C_nO^+, HC_nO^+, and OC_nO^+ ($n = 4 - 9$), as well as the IEs of their neutral counterparts, and are discussed in detail in the sections below.

Results indicate that the most stable isomers of C_nO^+, HC_nO^+, and OC_nO^+ ($n = 4 - 9$) are linear and possess either polyynic or cumulenic character. The most probable dissociation channel under the strong UV photon flux of the diffuse ISM is the loss of a CO unit, with BDEs being larger for cumulenic structures. Thus, the species with the greatest chance to survive in the diffuse ISM are cumulenic. Photoionization of the cations to form the dications can be neglected (except in H II regions) since most of the second ionization energies are larger than 13.6 eV. The IEs of all neutral species are in a photon energy range that should facilitate production of C_nO^+, HC_nO^+, and OC_nO^+ in the ISM.

3.1 C_nO^+

The most stable forms of C_nO^+ species are linear. C_7O^+ has the peculiarity of being bent (as previously found by Joseph et al. (2013)) whereby the terminal carbon atom deviates from linearity by $\sim 10°$, as shown in Figure 1. The valence orbital configurations of C_nO^+ are $(\sigma)^2(\pi)^3$ and $(\pi)^1$ for even and odd numbers of carbon atoms, respectively, leading to $^2\Pi$ electronic ground states. Bond dissociation energies of C_nO^+ are presented in Table 1. As expected, the lowest dissociation channel corresponds to CO loss. The energy required to release a CO unit ranges from 4.47 eV to 2.76 eV, decreasing in a non-monotonic fashion from C_4O^+ to C_9O^+. The calculated potential energy surfaces along the CO-loss coordinate predict that the dissociation is barrierless for all C_nO^+ species. IEs are listed in Table 1 and show a decrease as the chain lengthens. An oscillation pattern is observed, reflecting the alternation of singlet and triplet spin multiplicity in the electronic ground state of the neutral and doubly ionized species.

Table 1. Lowest bond dissociation energies (BDEs) corresponding to the loss of a CO unit from C_nO^+, HC_nO^+, and OC_nO^+. Ionization energies (IEs) of the corresponding neutral counterparts (C_nO, HC_nO, and OC_nO) and of the singly-charged cations. All energies are given in eV. Calculations were performed at the CCSD(T)/cc-pVTZ//ωB97X-D/cc-pVDZ level of theory.

n	C_nO^+ $BDE_{(-CO)}$	C_nO IE	C_nO^+ IE	HC_nO^+ $BDE_{(-CO)}$	HC_nO IE	HC_nO^+ IE	OC_nO^+ $BDE_{(-CO)}$	OC_nO IE	OC_nO^+ IE
4	4.47	9.48	15.99	4.05	8.78	16.13	3.45	8.33	14.21
5	3.73	10.33	16.64	5.38	6.89	16.31	3.35	9.24	15.74
6	3.30	8.67	13.95	3.77	8.23	14.21	2.75	7.74	12.59
7	3.28	9.47	14.69	4.61	6.65	14.71	2.97	8.54	13.94
8	3.18	8.14	12.58	3.73	7.84	12.92	3.02	7.38	11.50
9	2.76	9.05	13.19	4.15	6.43	13.65	2.73	8.14	12.70

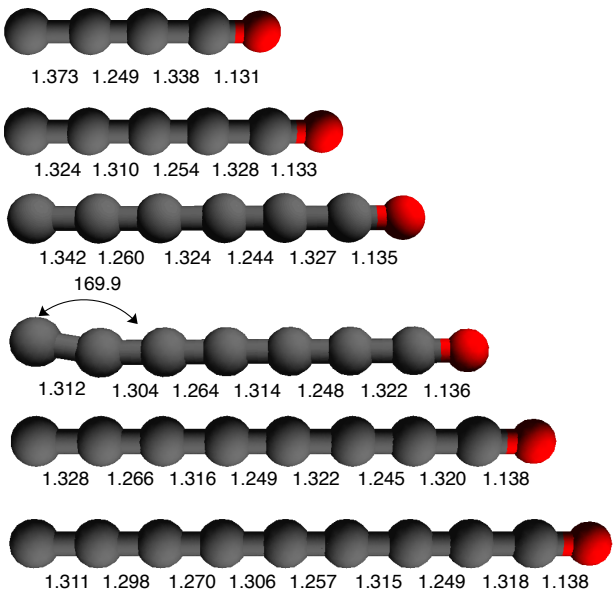

Figure 1. Optimized geometries of the lowest-lying C_nO^+ isomers at the ωB97X-D/cc-pVDZ level of theory. All species are linear expect C_7O^+. Bond lengths are in Å, angle (for C_7O^+) in degrees.

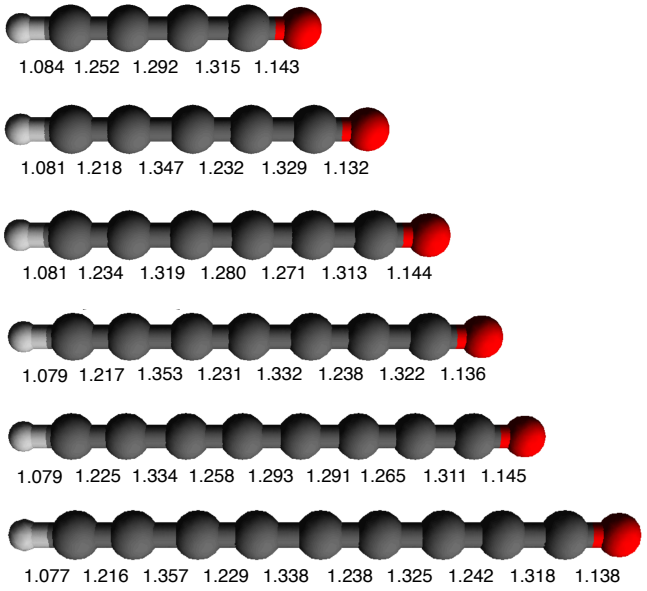

Figure 2. Optimized geometries of the lowest-lying HC_nO^+ isomers at the ωB97X-D/cc-pVDZ level of theory. Bond lengths are in Å.

3.2 HC_nO^+

The most stable HC_nO^+ isomers are linear structures with the carbon chain terminated on each end by O and H atoms (see Figure 2). The valence orbital configuration of HC_nO^+ are $(\pi)^2$ ($^3\Sigma$ symmetry electronic ground states) and $(\pi)^4$ ($^1\Sigma$ symmetry electronic ground states) for even and odd number of carbon atoms, respectively. Lowest dissociation energies of HC_nO^+ are given in Table 1, corresponding to CO loss channels. BDEs decrease with increasing chain length. BDEs are generally larger for species with odd number of carbon atoms, reflecting the cumulenic-type stability of these species as opposed to polyyne-like structure for even number of carbon atoms. IEs of HC_nO and HC_nO^+ are summarized in Table 1. Larger first ionization energies and smaller second ionization energies are observed for even number of carbon and vice-versa for the odd number of carbon atoms, reflecting the alternation of cumulene- and polyyne-type structures

3.3 OC_nO^+

The most stable OC_nO^+ isomer is a linear carbon chain terminated by one O atom at each end (see Figure 3). Linear OC_nO^+ molecules have electronic ground states of $^2\Pi$ symmetry. BDEs generally decrease with the length of the carbon chain, as can be seen in Table 1. The higher BDEs for the $OC_{2n+1}O^+$ reflect their cumulenic nature as proposed by Hardy et al. (2016). The first and second ionization energies of OC_nO are given in Table 1 and exhibit similar behaviour to C_nO.

4 OPTICAL PROPERTIES

To assess the possibility of detecting C_nO^+, HC_nO^+, and OC_nO^+ ($n = 4 - 9$) in the diffuse ISM through electronic spectroscopy, their vertical excitation energies and corresponding oscillator strengths have been computed.

4.1 C_nO^+

Experimental information on electronic excitations of C_nO^+ ($n > 3$) is limited to a single electronic transition of C_7O^+, observed in a Ne matrix at 276 nm and assigned to the $4\,^2\Sigma^+ \leftarrow \tilde{X}\,^2\Sigma^+$ excitation. Our calculations predict that the electronic ground state of C_7O^+ has Π symmetry and that the observed absorption is a $\Pi \leftarrow \Pi$ transition with an associated oscillator strength (f) of 2.9. Our calculations

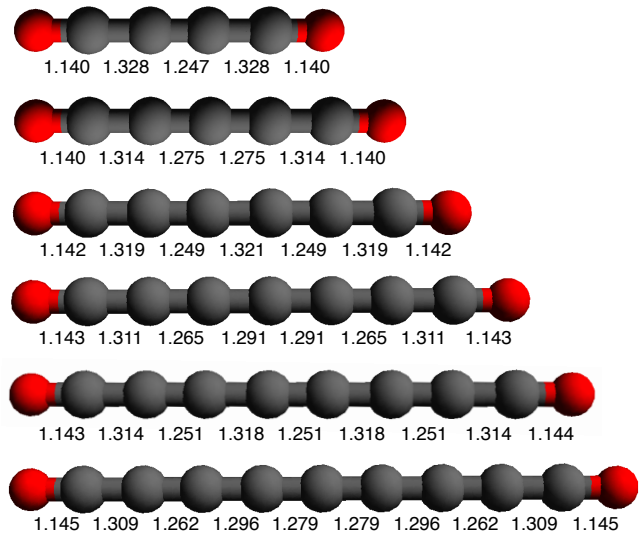

Figure 3. Optimized geometries of the lowest-lying OC_nO^+ isomers at the ωB97X-D/cc-pVDZ level of theory. Bond lengths are in Å.

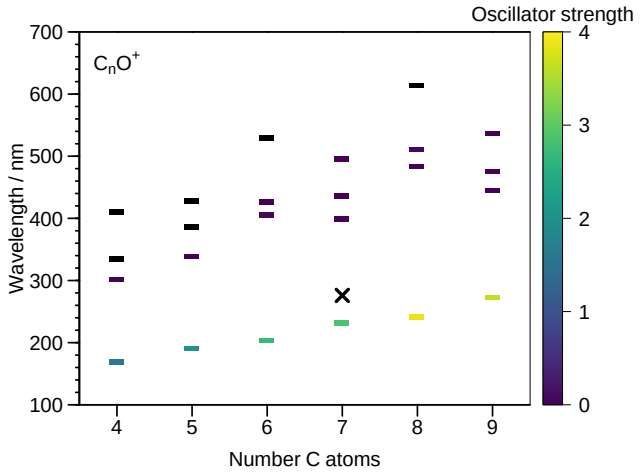

Figure 4. Vertical electronic excitation wavelengths and oscillator strengths for the first three $\Pi \leftarrow \Pi$ transitions of C_nO^+. The most intense $\Pi \leftarrow \Pi$ transitions occur in the UV region. Calculations are obtained at the EOM-CCSD/cc-pVTZ level of theory. The black cross represents the experimental adiabatic excitation energy of C_7O^+ reported by Joseph et al. (2013).

revealed other transitions in the UV at 295, 276, and 248 nm with oscillator strengths of 6.6×10^{-3} , 4.2×10^{-3}, and 8.4×10^{-3}, respectively. These transitions have similar, if not lower, intensities than those calculated in the visible (reported in Table 2) and because no transitions were experimentally observed in the visible spectral region by Joseph et al. (2013), we assume that the transition with f = 2.9 dominates the absorption features observed experimentally.

The C_nO^+ vertical excitation wavelengths and their corresponding oscillator strengths were obtained at EOM-CCSD level of theory. The results for the first three $\Pi \leftarrow \Pi$ transitions and of the most intense $\Pi \leftarrow \Pi$ transitions in the UV are displayed in Figure 4 and summarized in Table 2. The black cross in Figure 4 represents the experimental adiabatic electronic excitation wavelength from Joseph et al. (2013) for C_7O^+. The calculated vertical electronic excitation

C_nO^+	$\lambda_{vert.}$ / nm ($\lambda_{adia.,exp}$)	f ($\times 10^{-2}$)
4	412.4	0.04
	335.9	0.01
	302.7	3.1
	170.3	160
5	429.5	0.38
	387.0	0.23
	340.2	0.81
	192.5	210
6	530.8	0.16
	428.3	0.53
	406.6	6.1
	205.0	270
7	499.2	1.4
	442.7	0.56
	401.8	1.5
	232.9 (276.0)	290
8	614.5	0.38
	511.5	7.9
	485.5	3.0
	243.3	390
9	537.7	2.7
	477.1	0.82
	445.8	2.0
	274.5	360

Table 2. Vertical electronic excitation wavelengths ($\lambda_{vert.}$) and oscillator strengths (f) of the first three $\Pi \leftarrow \Pi$ transitions and of the most intense $\Pi \leftarrow \Pi$ transitions for C_nO^+ in the UV region. Calculations are obtained at the EOM-CCSD/cc-pVTZ level of theory. Experimental adiabatic excitation energy ($\lambda_{adia.,exp}$) value for C_7O^+ taken from Joseph et al. (2013).

wavelengths of the C_nO^+ show a linear dependency for n even and n odd, respectively. The oscillator strengths of the electronic transitions in the visible spectral range are small and thus these transitions could only contribute to weak DIBs. Some transitions are calculated with very large oscillator strengths (1.6 to 3.9), however, these strong transitions occur in the deep UV spectral region and are thus unlikely to be associated with commonly known DIBs.

4.2 HC_nO^+

The only experimental data for electronic excitations of HC_nO^+ are the matrix spectroscopy measurements of HC_7O^+ (Chakraborty et al. 2016). The spectrum consists of one band system assigned to the $2^1\Sigma^+ \leftarrow \tilde{X}^1\Sigma^+$ transition with its origin band located at 278.0 nm. Our calculations are consistent with this assignment, as the transition is predicted to be strong (f=2.6) with a vertical excitation wavelength of 224.4 nm.

Calculated vertical excitation wavelengths for HC_nO^+ and their corresponding oscillator strengths are presented in Figure 5 and summarized in Table 3 (for HC_9O^+ a cc-pVDZ basis set was used instead of cc-pVTZ due to convergence problems). Two linear trends are observed for the transition wavelengths, with one corresponding to chains with an odd number of carbon atoms and the other to chains with an even number of carbon atoms. For odd n chains, the wavelengths are associated with the promotion of an electron from the highest occupied molecular orbital (HOMO) to the lowest unoccupied molecular orbital (LUMO). For even n chains, the wavelengths are associated with the promotion of an electron from the orbital be-

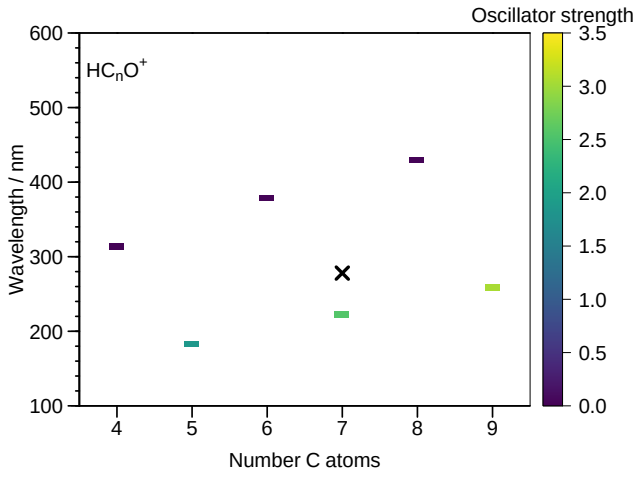

Figure 5. Vertical electronic excitation wavelengths and oscillator strengths of the first dipole-allowed $\Sigma \leftarrow \Sigma$ transitions for HC_nO^+. Calculations are obtained at the EOM-CCSD/cc-pVTZ level of theory. Note that for HC_9O^+, EOM-CCSD/cc-pVDZ was used. The black cross represents the experimental value of the adiabatic excitation energy for HC_7O^+ reported by Chakraborty et al. (2016).

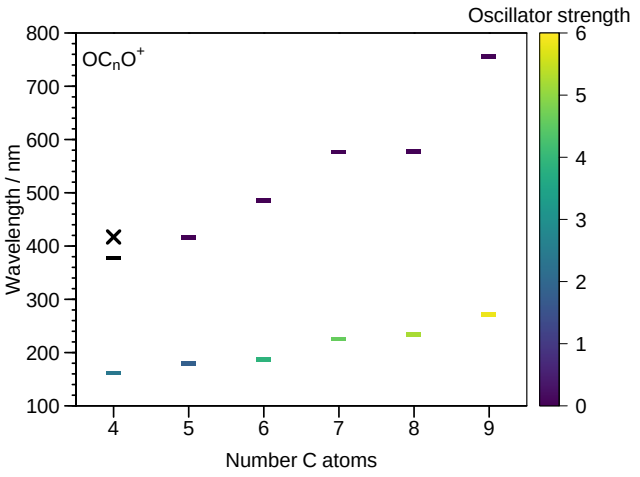

Figure 6. Vertical electronic excitation wavelengths and oscillator strength of the first $\Pi \leftarrow \Pi$ dipole-allowed transitions and of the most intense $\Pi \leftarrow \Pi$ transition in the UV for OC_nO^+. Calculations are obtained at the EOM-CCSD/cc-pVTZ level of theory. The black cross represents the experimental value of the adiabatic energy for OC_4O^+ reported by Hardy et al. (2016).

HC_nO^+	$\lambda_{vert.}$ / nm ($\lambda_{adia.,exp}$)	f ($\times 10^{-2}$)
4 (triplet)	314.9	2.4
5 (singlet)	183.9	190
6 (triplet)	379.8	2.9
7 (singlet)	224.4 (278.0)	260
8 (triplet)	431.0	3.4
9 (singlet)	260.0	300

Table 3. Vertical electronic excitation energies ($\lambda_{vert.}$) and oscillator strengths (f) of the lowest dipole-allowed transitions for HC_nO^+ calculated using EOM-CCSD method. Experimental adiabatic excitation energy ($\lambda_{adia.,exp}$) value for HC_7O^+ taken from Chakraborty et al. (2016).

OC_nO^+	$\lambda_{vert.}$ / nm ($\lambda_{adia.,exp}$)	f ($\times 10^{-2}$)
4	378.7 (417.3)	0.36
	163.0	240
5	416.9	1.4
	193.7	150
6	486.9	0.87
	199.5	390
7	578.3	3.0
	226.6	460
8	579.4	4.4
	236.0	520
9	758.3	5.8
	263.2	580

Table 4. Vertical Electronic excitation wavelengths ($\lambda_{vert.}$) and Oscillator Strengths f of the first $\Pi \leftarrow \Pi$ dipole-allowed transitions and of the most intense $\Pi \leftarrow \Pi$ transition in the UV for OC_nO^+. Calculations are obtained at the EOM-CCSD/cc-pVTZ level of theory. Experimental adiabatic energy ($\lambda_{adia.,exp}$) value for OC_4O^+ taken from Hardy et al. (2016)

low the single occupied molecular orbital (SOMO-1) to the SOMO. The experimental adiabatic excitation wavelength for HC_7O^+ from Chakraborty et al. (2016) is denoted in Figure 5 with a black cross.

The oscillator strengths presented in Figure 5 indicate that the electronic transitions for HC_nO^+ with odd n are expected to be two orders of magnitude stronger than for HC_nO^+ with even n. The strong transitions of HC_nO^+ with odd n are too deep in the UV to account for the main known DIBs. Electronic transitions for HC_nO^+ with even n occur in the visible but are weak, indicating that the column densities for HC_nO^+ with even n must be fairly large to account for DIBs.

4.3 OC_nO^+

The electronic spectrum of OC_4O^+ has been measured in a neon matrix and in the gas phase by Hardy et al. (2016), with its $1^2\Pi_u \leftarrow \tilde{X}^2\Pi_u$ origin transition occurring at 413.2 nm. Our calculations, which predict a transition at 378.7 nm, are consistent with the experimental observations and assignment of the transition. A significantly stronger $\Pi \leftarrow \Pi$ transition (f=2.4) is predicted to occur far deeper into the UV (163.0 nm), beyond the range that was investigated in the previous study.

The vertical electronic excitation wavelengths and oscillator strengths calculated at the EOM-CCSD/cc-pVTZ level of theory for the first $\Pi \leftarrow \Pi$ dipole-allowed transition and the most intense $\Pi \leftarrow \Pi$ transition in the UV are presented in Figure 6 and Table 4. Similar to C_nO^+, the calculated vertical excitation wavelengths of OC_nO^+ show roughly linear dependencies on the chain length for both even and odd n cations. The electronic transitions in the visible spectral range are expected to be weak and could probably only contribute to weak DIBs. The strong, higher energy transitions are outside the appropriate spectral range to be considered for DIBs, although become promising candidates for larger OC_nO^+ species not investigated in the current work.

Table 5. Reactions of carbon chain cations with O(^{3}P) atom and CO molecule. Energies are given in eV. Calculations performed at the CCSD(T)/cc-pVTZ//ωB97X-D/cc-pVDZ level of theory. Spin multiplicities are given in brackets.

Reactants	Adducts, $\Delta_r H^0$ / eV
$C_4^+(2)$ + O	$C_4O^+(2)$, −8.20
$C_5^+(2)$ + O	$C_5O^+(2)$, −7.66
$C_6^+(2)$ + O	$C_6O^+(2)$, −7.90
$C_7^+(2)$ + O	$C_7O^+(2)$, −7.67
$C_8^+(2)$ + O	$C_8O^+(2)$, −7.70
$C_9^+(2)$ + O	$C_9O^+(2)$, −7.41
$C_3^+(2)$ + CO	$C_4O^+(2)$, −4.47
$C_4^+(2)$ + CO	$C_5O^+(2)$, −3.73
$C_5^+(2)$ + CO	$C_6O^+(2)$, −3.30
$C_6^+(2)$ + CO	$C_7O^+(2)$, −3.28
$C_7^+(2)$ + CO	$C_8O^+(2)$, −3.18
$C_8^+(2)$ + CO	$C_9O^+(2)$, −2.76

5 ION–NEUTRAL REACTIONS

Ion–neutral reactions are the most likely bottom-up formation mechanisms for oxygenated carbon chain cations in the diffuse ISM. Here, we explore reactions between C_n^+, HC_n^+, and C_nO^+ cations and some of the most abundant neutral species available (O, H, H_2, and CO). Only the addition of O and CO can generate O-bearing carbon chains; the addition of H and H_2 are investigated as possible routes to form HC_nO^+ species from already existing cationic oxygenated molecules. Other possible reactions, not considered here, involve addition of HCO^+, H_2CO, and CH_3OH. These species are several orders of magnitude less abundant than O and CO; their low collision rates are unlikely to yield a sufficient population of oxygenated carbon chain cations to account for DIBs (Snow & McCall 2006).

The results of our calculations, discussed in further detail for each cation below, suggest that atomic additions of O or H are too exothermic to form stabilized C_nO^+, HC_nO^+, and OC_nO^+ (n = 4 – 9). Addition of CO to cationic carbon chains is a more promising mechanism to form C_nO^+, HC_nO^+, and OC_nO^+ (n = 4 – 9), as is the addition of H_2 to C_nO^+ to form HC_nO^+. C_nO^+, HC_nO^+, and OC_nO^+ can exist as various isomers, although their large internal energies following formation, and the improbability to radiatively stabilize, indicate that dissociation processes should dominate.

5.1 C_nO^+

Both O(^{3}P) and CO may react with C_n^+ (n = 4 – 9) to produce C_nO^+ cations in the doublet and quartet states. Only the channels leading to the most stable structure (doublet) are investigated, with the results summarized in Table 5. These reactions are spin-allowed and have barrierless entrance channels. The reaction enthalpies, calculated at the CCSD(T)/cc-pVTZ//ωB97X-D/cc-pVDZ level of theory, are significantly larger in magnitude (from −7.41 to −8.20 eV) than the BDEs involving CO loss (from 2.76 to 4.47 eV; see Table 1), indicating that dissociation of the highly excited adducts is likely to occur as they dissipate excess energy. The addition of a CO molecule to C_n^+ requires stabilisation of the adduct to avoid the reverse (dissociation) reaction. However, radiative stabilization is only expected to occur for larger carbon clusters, based on observations by Sun et al. (1993) of ion–neutral reactions involving C_n^+ with $n \geq 10$. Therefore, C_nO^+ is most likely a transient species.

Table 6. Formation of HC_nO^+ through reactions of linear C_nO^+ with H(^{2}S) atom and H_2 molecule and reaction of HC_3^+ with CO. Energies are given in eV. Calculations performed at CCSD(T)/cc-pVTZ//ωB97X-D/cc-pVDZ level of theory. Spin multiplicities are given in brackets.

Reactants	Adducts, $\Delta_r H^0$ / eV	Products, $\Delta_r H^0$ / eV
$C_4O^+(2)$ + H	$HC_4O^+(3)$, −5.15	
$C_5O^+(2)$ + H	$HC_5O^+(1)$, −6.59	
$C_6O^+(2)$ + H	$HC_6O^+(3)$, −5.01	
$C_7O^+(2)$ + H	$HC_7O^+(1)$, −6.31	
$C_8O^+(2)$ + H	$HC_8O^+(3)$, −4.93	
$C_9O^+(2)$ + H	$HC_9O^+(1)$, −6.31	
$C_4O^+(2)$ + H_2	$H_2C_4O^+(2)$, −4.87	$HC_4O^+(3)$ + H, −0.74
$C_5O^+(2)$ + H_2	$H_2C_5O^+(2)$, −4.43	$HC_5O^+(1)$ + H, −2.17
$C_6O^+(2)$ + H_2	$H_2C_6O^+(2)$, −4.36	$HC_6O^+(3)$ + H, −0.58
$C_7O^+(2)$ + H_2	$H_2C_7O^+(2)$, −4.12	$HC_7O^+(1)$ + H, −1.89
$C_8O^+(2)$ + H_2	$H_2C_8O^+(2)$, −4.02	$HC_8O^+(3)$ + H, −0.50
$C_9O^+(2)$ + H_2	$H_2C_9O^+(2)$, −4.02	$HC_9O^+(1)$ + H, −1.89
$HC_3^+(2)$ + CO	$HC_4O^+(3)$, −4.05	
$HC_4^+(2)$ + CO	$HC_5O^+(1)$, −5.38	
$HC_5^+(2)$ + CO	$HC_6O^+(3)$, −3.77	
$HC_6^+(2)$ + CO	$HC_7O^+(1)$, −4.61	
$HC_7^+(2)$ + CO	$HC_8O^+(3)$, −3.73	
$HC_8^+(2)$ + CO	$HC_9O^+(1)$, −4.15	

5.2 HC_nO^+

Energies associated with the reactions of C_nO^+ (n = 4 – 9) with H and H_2, and between HC_n^+ and CO, have been calculated to elucidate possible formation pathways of HC_nO^+ cations. Our calculations indicate that the addition of H to C_nO^+ is barrierless, similar to the case of O addition to C_n^+ as described above. The internal energy of HC_nO^+ (see Table 6) following the addition of H is much larger than the energy needed to access the CO-dissociation channel, and therefore this pathway is not conducive to HC_nO^+ formation in an isolated environment.

Reactions of molecular hydrogen with C_nO^+ occur through a two-step mechanism as depicted in Figure 7 for C_4O^+. The exothermic addition of H_2 (see Table 6) yields excited $H_2C_nO^+$ adducts, which subsequently undergo unimolecular dissociation along the H loss coordinate. The HC_nO^+ molecules retain between 0.50 and 2.17 eV of excess energy, which is insufficient to detach CO (Table 1). Formation of HC_nO^+ through the C_nO^+ + H_2 ion–neutral reaction is thus a possible route in the diffuse ISM.

The addition of a CO molecule to HC_n^+ is similar to the addition to C_n^+ and C_nO^+, where the high internal energies of the adducts facilitate their destruction through dissociation or possibly isomerization. Note that the HC_{n-1}^+ + CO → HC_nO^+ reaction has been considered by Cernicharo et al. (2021) to explain the abundances of oxygenated carbon chains detected in TMC-1. Their model could reproduce some of the observed features but greatly overestimate the abundances of molecules such as C_5O, HC_4O, and HC_6O.

5.3 OC_nO^+

Addition of O and CO to C_nO^+ and $C_{n-1}O^+$, respectively, have been considered to form OC_nO^+. The lowest energy pathways for these reactions are spin allowed and have no entrance barriers. The CO addition channel is a significantly more competitive pathway, based on the large exothermicity of the O addition channel. Enthalpies for both sets of reactions are given in Table 7.

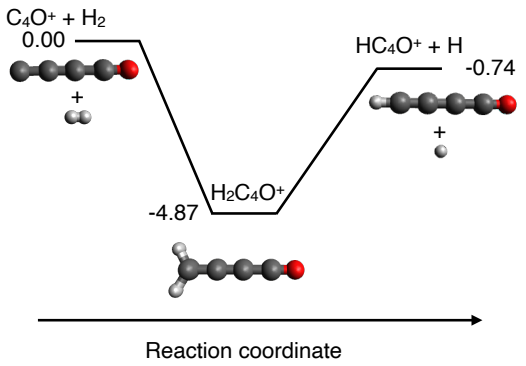

Figure 7. Reaction coordinate scheme for $C_4O^+ + H_2$.

Table 7. Reactions of linear C_nO^+ with atomic oxygen and carbon monoxide. Energies are given in eV. Calculations were performed at the CCSD(T)/cc-pVTZ//ωB97X-D/cc-pVDZ level of theory. Spin multiplicities are given in brackets.

Reactants	Adducts, Δ_rH^0 / eV
$C_4O^+(2) + O(3)$	$OC_4O^+(2)$, −7.74
$C_5O^+(2) + O(3)$	$OC_5O^+(2)$, −7.83
$C_6O^+(2) + O(3)$	$OC_6O^+(2)$, −8.70
$C_7O^+(2) + O(3)$	$OC_7O^+(2)$, −8.75
$C_8O^+(2) + O(3)$	$OC_8O^+(2)$, −8.60
$C_9O^+(2) + O(3)$	$OC_9O^+(2)$, −8.60
$C_3O^+(2) + CO(1)$	$OC_4O^+(2)$, −3.45
$C_4O^+(2) + CO(1)$	$OC_5O^+(2)$, −3.35
$C_5O^+(2) + CO(1)$	$OC_6O^+(2)$, −2.75
$C_6O^+(2) + CO(1)$	$OC_7O^+(2)$, −2.97
$C_7O^+(2) + CO(1)$	$OC_8O^+(2)$, −3.02
$C_8O^+(2) + CO(1)$	$OC_9O^+(2)$, −2.73

6 ASTROPHYSICAL IMPLICATIONS

In dense molecular clouds such as TMC-1, cyano-polyynes and oxygentated carbon chains have been detected with typical column densities of 10^{11} to 10^{13} molecules per cm^2 (McGuire et al. 2017; Cordiner et al. 2017). Species with low abundances in the diffuse ISM could still be considered as DIB carriers by compensating the low abundances by large electronic oscillator strengths. If one assumes a molecule where most of the electronic transition intensity is carried in the origin band rather than distributed over many vibronic transitions, then, for typical weak DIBs with an observed equivalent width of $\approx$ 10 mÅ/E(B-V) mag where E(B-V) is the reddening of the interstellar object defined as the difference between the observed color index and the true color index of the object and using the carbon abundance of the interstellar gas as $\chi_C = N_C/N_H = 1.4 \times 10^{-4}$, one can derive (see Cami (2014); Omont (2016))

$$\chi_{CM} \times f \approx 10^{-6}, \quad (1)$$

where χ_{CM} is the fraction of total interstellar carbon locked up in the DIB carrier candidate (M), and f is the oscillator strength of the electronic transition of M. The column densities (N) per E(B-V) can be expressed in cm^{-2}/mag by adapting the formula given by Hardy et al. (2016)

$$\frac{N(\mathrm{cm}^{-2})}{E(\mathrm{B-V})} = 1.13 \times 10^{20} \frac{\mathrm{EW(Å/mag)}}{\lambda(\mathrm{Å})^2 \times f}, \quad (2)$$

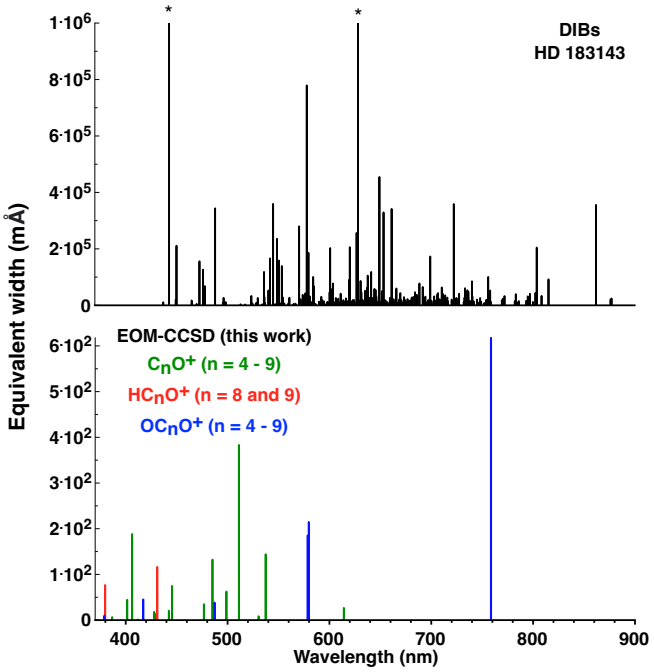

Figure 8. Comparison of the DIB spectrum observed towards HD 143183 with the equivalent widths for oxygenated cationic carbon clusters. Equivalent widths calculated using *ab initio* vertical excitation wavelengths and oscillator strengths while assuming a column density of 2×10^{13} molecules per cm^2 and an E(B-V) of 1.27 (Hobbs et al. 2009). The asterisked DIBs are truncated for clarity.

with EW being the equivalent width of the DIB of interest and λ its corresponding wavelength.

Table 8 summarizes the amount of carbon in the ISM (χ_{CM}) needed to be locked up in C_nO^+, HC_nO^+, and OC_nO^+, as well as the column densities ($N_M$cm^{-2}/mag), necessary for these cations to give rise to a DIB with an equivalent width of 10 mÅ/mag. For example, the estimated column density of C_{60}^+ is of 2×10^{13} cm^{-2} and the ratio of interstellar carbon locked into C_{60}^+ is estimated to be (2-4) $\times 10^{-4}$, assuming an average equivalent width of 300 mÅ/mag (Walker et al. 2015; Strelnikov et al. 2015; Omont 2016).

Assuming a column density of 2×10^{13} molecules per cm^2, an E(B-V) of 1.27 (Hobbs et al. 2009), and that the intensities of transitions are concentrated in the origin band, the vertical excitations of C_nO^+, HC_nO^+, and O_nO^+ cations can be compared with the DIB spectrum observed towards HD 143183 (Hobbs et al. 2009) as shown in Figure 8. The figure only serves as a guide to indicate the spectral region where the three different families of oxygenated chains are expected to absorb compared to absorption bands of DIBs; the calculations do not have the precision required to make direct comparisons.

6.1 C_nO^+

The observed column densities or upper limits for C_nO species in TMC-1 are 1.5×10^{12}, 1.5×10^{12}, $< 1.2 \times 10^{11}$, and 4.0×10^{10} cm^{-2} for C_2O, C_3O, C_4O, and C_5O, respectively (Cernicharo, J. et al. 2020) for a column density along the TMC-1 line of sight of $n_{H_2} = 10^{22}$ H_2 per cm^2 (Gratier et al. 2016), which corresponds to an E(B-V) of $\approx$ 3.2. These values can probably be taken as upper limits of column densities that could be found in space for such species, with dense clouds likely to be the most propitious medium to grow complex

C_nO^+	$\lambda_{vert.}$ / nm	f ($\times10^{-2}$)	χ_{CM} ($\times10^{-5}$)	N_M [cm^{-2}/mag] ($\times10^{12}$)
4	412.4	0.04	200	< 200
5	429.5	0.38	30	< 20
	387.0	0.23	40	< 40
6	530.8	0.16	60	< 30
	428.3	0.53	20	< 20
	406.6	6.1	2	< 3
7	499.2	1.4	7	< 4
	442.7	0.56	20	< 20
	401.8	1.5	7	< 5
8	614.5	0.38	30	< 8
	511.5	7.9	1	< 0.6
	485.5	3.0	3	< 2
9	537.7	2.7	4	< 2
	477.1	0.82	1	< 7
	445.8	2.0	4	< 3
HC_nO^+	$\lambda_{vert.}$ / nm	f ($\times10^{-2}$)	χ_{CM} ($\times10^{-5}$)	N_M [cm^{-2}/mag] ($\times10^{12}$)
6 (triplet)	379.8	2.9	3	< 3
8 (triplet)	431.0	3.4	3	< 2
OC_nO^+	$\lambda_{vert.}$ / nm	f ($\times10^{-2}$)	χ_{CM}($\times10^{-5}$)	N_M [cm^{-2}/mag] ($\times10^{12}$)
4	378.7	0.36	30	< 30
5	416.9	1.4	7	< 5
6	486.9	0.87	10	< 6
7	578.3	3.0	3	< 2
8	579.4	3.4	3	< 1
9	758.3	5.8	2	< 0.4

Table 8. Fraction of total interstellar carbon locked up in cationic oxygenated carbon chains (χ_{CM}) and estimated minimal column density (N_M) to explain DIBs with equivalent width of 10 mÅ/mag with the $\lambda_{vert.}$ and f calculated previously. Only electronic transitions calculated above 350 nm are considered.

organic molecules (COMs). Additionally, it is hard to anticipate the proportion of the C_nO species that would be ionized in the diffuse ISM. Considering bottom-up mechanisms for the formation of these species, it is unlikely that linear C_nO^+ species are DIBs carriers.

6.2 HC_nO^+

In the HC_nO^+ family, only HC_6O^+ and HC_8O^+ possess electronic transitions in the spectral region relevant to DIBs. Their respective χ_{CM} and N_M are presented in Table 8. Based on these numbers, only HC_6O^+ and HC_8O^+ present as possible DIBs carriers. Closed-shell carbon-based chains with up to 11 carbon atoms have been detected in space Loomis et al. (2021) but open-shell carbon-based chains remain undetected. Chains with odd numbers of electrons such as HC_6O^+ and HC_8O^+, typically possess a triplet spin multiplicity in their most stable form. Studies have implied that these molecules remain undetected due to searches being carried out for the singlet states rather than the triplet states (Bâldea 2019b; Bâldea 2019a). It is hopeful that the calculations presented for triplet HC_6O^+ and HC_8O^+ aid in their possible detection despite their high reactivity owing to the unpaired electron.

6.3 OC_nO^+

The χ_{CM} and N_M of OC_nO^+ species to account for DIBs with an equivalent width of 10 mÅ/mag are given in Table 8. The ratio of interstellar carbon to be locked up in OC_nO^+ as well as the column densities needed to explain DIBs with equivalent widths of 10 mÅ/mag are reasonable. Among all species considered in the present study, OC_4O^+ is the only one with a known gas phase electronic spectrum (Hardy et al. 2016), the bands of which do not coincide with any known DIBs. As pointed out by Hardy et al. (2016) oxygenated carbon chains are typically more sensitive to photodestruction than hydrocarbons because of the low CO dissociation threshold. However, cumulenic structures such as $OC_{2n+1}O^+$ have larger photodestruction thresholds and can more easily redistribute energy into vibrational degrees of freedom after electronic excitation. Considering this, OC_9O^+ is the most promising candidate among OC_nO^+ species investigated in this work. However, if we assume absorption of a 10 eV photon and estimate the vibrational temperature (T_v) using $E_{h\nu} = (3N - 5)k_bT_v$ with N being the number of atoms, we find the temperature ($T_v \sim 4150$ K) is too high for OC_9O^+ to survive in the diffuse ISM. Furthermore, OC_9O^+ has its expected electronic transition occurring at a minimum wavelength of 758.3 nm, which is beyond the densest spectral region of the DIBs (550 to 750 nm) as can be seen in Figure 8. Therefore, even OC_9O^+ does not appear as

such a promising DIB candidate. Nevertheless, similar to their bare carbon cumulene counterparts,Fischer & Maier (1997); Maier et al. (2004) the O-bearing carbon chains possess large f values. Although these high f-values reported presently for chains from 5 to 11 atoms are in the UV, these high f-values can be extrapolated to the visible spectral domain as the number of carbon increases, as it can be seen in Figures 4, 5, and 6. Therefore, longer oxygenated chains should be the first candidates for laboratory studies and subsequent astronomical searches, as they will additionally have greater chance to survive in the diffuse ISM.

The column density in the diffuse ISM is challenging to estimate due to the lack of information on formation mechanisms of COMs. In dense molecular clouds, the ratios OC_nO to C_nO and HC_nO remain unknown since OC_nO are centro-symmetric molecules and thus escape radioastronomy detection. Yet, the detection of several C_nO and $HC_nO^{(+)}$ species allude to the presence of OC_nO and possibly OC_nO^+ species in space.

7 CONCLUSIONS

In this paper we assess the potential role of cationic oxygenated carbon chains (C_nO^+, HC_nO^+, and OC_nO^+ with $n = 4-9$) as carriers to the DIBs. As excitation wavelengths increase with lengthening of the chains, chains with more than 9 carbon atoms not only have a better chance of surviving in the ISM but will also have wavelengths excitations in the densest region of the DIB spectrum. Although C_nO^+, HC_nO^+, and OC_nO^+ for $n = 4-9$ possess spectral signatures that could contribute to the DIB spectra, it is unclear if these species could be formed in sufficient abundance due to the lack of information regarding their formation pathways in astrophysical media.

Based on the present calculations on the ion-neutral reactions leading to cationic oxygenated carbon chains, and on known column densities of neutral oxygenated carbon chains in TMC-1, additional formation mechanisms are necessary to build up a sufficient quantity of these species to account for DIBs. These mechanisms may include top-down reactions involving destruction of grains by UV, shocks, and cosmic rays. In addition, these reactions may generate higher energy, non-linear isomers that may exhibit greater photostabilities and stronger electronic transitions than linear chains.

ACKNOWLEDGEMENTS

U.J. thanks Evan J. Bieske, Marie-Aline Martin-Drumel and Olivier Pirali for beneficial discussions about the manuscript.

DATA AVAILABILITY

The data underlying this article will be shared on reasonable request to the corresponding author.

REFERENCES

Agúndez, Marcelino and Cernicharo, José and Guélin, Michel 2015, Astron. Astrophys., 577, L5
Bâldea I., 2019a, Adv. Theory Simul., 2, 1900084
Bâldea I., 2019b, Earth Space Chem., 3, 863
Bergin E., et al., 2000, Astrophys. J. Lett., 539, L129
Blanksby S. J., Bowie J. H., 1999, Mass Spectrom. Rev., 18, 131
Bohme D. K., Wl/odek S., Williams L., Forte L., Fox A., 1987, J. Chem. Phys., 87, 6934
Boogert A. A., Gerakines P. A., Whittet D. C., 2015, Annu. Rev. Astron. Astrophys., 53
Cami J., 2014, Proc. Int. Astron. Union, 9, 370
Campbell E. K., Holz M., Gerlich D., Maier J. P., 2015, Nature, 523, 322
Cernicharo, J. Marcelino, N. Agúndez, M. Endo, Y. Cabezas, C. Bermúdez, C. Tercero, B. de Vicente, P. 2020, Astron. Astrophys., 642, L17
Cernicharo J., Agundez M., Cabezas C., Tercero B., Marcelino N., Fuentetaja R., Pardo J., de Vicente P., 2021, Astron. Astrophys., 656, L21
Chai J.-D., Head-Gordon M., 2008, Phys. Chem. Chem. Phys.
Chakraborty A., Fulara J., Maier J. P., 2016, Mol. Phys., 114, 2794
Chen T., Zhen J., Wang Y., Linnartz H., Tielens A. G., 2018, Chem. Phys. Lett., 692, 298
Cordiner M., Charnley S., 2012, Astrophys. J., 749, 120
Cordiner M. A., Charnley S. B., Kisiel Z., McGuire B. A., Kuan Y.-J., 2017, Astrophys. J., 850, 187
Cuadrado S., Goicoechea J. R., Cernicharo J., Fuente A., Pety J., Tercero B., 2017, Astron. Astrophys., 603, A124
Dartois E., 2005, Space Sci. Rev., pp 293–310
Douglas A., 1977, Nature, 269, 130
Dunning T. H., 1989, J. Chem. Phys., 90, 1007
Eichelberger B., Snow T. P., Barckholtz C., Bierbaum V. M., 2007, Astrophys. J., 667, 1283
Fischer G., Maier J. P., 1997, Chem. Phys., 223, 149
Foing B., Ehrenfreund P., 1994, Nature, 369, 296
Frisch M. J., et al., 2016, Gaussian~16 Revision C.01
Goldsmith P. F., et al., 2000, Astrophys. J. Lett., 539, L123
Gratier P., Majumdar L., Ohishi M., Roueff E., Loison J., Hickson K., Wakelam V., 2016, Astrophys. J., Suppl. Ser., 225, 25
Hardy F.-X., Rice C., Chakraborty A., Fulara J., Maier J., 2016, Astrophys. J., 824, 9
Herbst E., Van Dishoeck E. F., 2009, Annu. Rev. Astron. Astrophys., 47, 427
Hincelin U., Wakelam V., Hersant F., Guilloteau S., Loison J., Honvault P., Troe J., 2011, Astron. Astrophys., 530, A61
Hobbs L., et al., 2009, Astrophys. J., 705, 32
Jenkins E. B., 2009, Astrophys. J., 700, 1299
Jin J., Li W., Liu Y., Wang G., Zhou M., 2017, J. Chem. Phys., 146, 214301
Joseph S. M., Fulara J., Garkusha I., Maier J. P., 2013, Mol. Phys., 111, 1977
Kowalski K., Piecuch P., 2001, J. Chem. Phys., 115, 643
Kroto H., Jura M., 1992, Astron. Astrophys., 263, 275
Kucharski S. A., Włoch M., Musiał M., Bartlett R. J., 2001, J. Chem. Phys., 115, 8263
Larsson B., et al., 2007, Astron. Astrophys., 466, 999
Li W., Jin J.-y., Qu H., Wang G.-j., Zhou M.-f., 2019, Chin. J. Chem. Phys., 32, 77
Loomis R. A., et al., 2021, Nat. Astron., 5, 188
Maier J. P., Walker G. A., Bohlender D. A., 2004, Astrophys. J., 602, 286
Matthews H. E., Irvine W. M., Friberg P., Brown R. D., Godfrey P. D., 1984, Nature, 310, 125
McGuire B. A., Burkhardt A. M., Shingledecker C. N., Kalenskii S. V., Herbst E., Remijan A. J., McCarthy M. C., 2017, Astrophys. J. Lett., 843, L28
Nagarajan R., Maier J. P., 2010, Int. Rev. Phys. Chem., 29, 521
Noble J., Fraser H., Aikawa Y., Pontoppidan K., Sakon I., 2013, Astrophys. J., 775, 85
Öberg K. I., Boogert A. A., Pontoppidan K. M., Van den Broek S., Van Dishoeck E. F., Bottinelli S., Blake G. A., Evans II N. J., 2011, Astrophys. J., 740, 109
Ohishi M., et al., 1991, Astrophys. J., 380, L39
Omont A., 2016, Astron. Astrophys., 590, A52
Palumbo M., Leto P., Siringo C., Trigilio C., 2008, Astrophys. J., 685, 1033
Pety J., et al., 2012, Astron. Astrophys., 548, A68
Quan D., Herbst E., Millar T., Hassel G. E., Lin S. Y., Guo H., Honvault P., Xie D., 2008, Astrophys. J., 681, 1318
Riplinger C., Sandhoefer B., Hansen A., Neese F., 2013, J. Chem. Phys., 139, 134101
Sarre P., 2019, Mon. Notices Royal Astron. Soc., 490, L17
Snow T. P., McCall B. J., 2006, Annu. Rev. Astron. Astrophys., 44, 367
Strelnikov D., Kern B., Kappes M., 2015, Astron. Astrophys., 584, A55
Sun J., Gruetzmacher H. F., Lifshitz C., 1993, J. Am. Chem. Soc., 115, 8382

Van der Zwet G., Allamandola L., 1985, Astron. Astrophys., 146, 76
Walker G., Bohlender D., Maier J., Campbell E., 2015, Astrophys. J. Lett., 812, L8
Whittet D., 2010, Astrophys. J., 710, 1009
Wirström E. S., Charnley S. B., Cordiner M. A., Ceccarelli C., 2016, Astrophys. J., 830, 102
Yang Z., Snow T. P., Bierbaum V. M., 2010, Phys. Chem. Chem. Phys., 12, 13091

This paper has been typeset from a TEX/LATEX file prepared by the author.